Optical control of adenosine A_3 receptor function in psoriasis

Marc López-Cano[1,2], **Ingrid Filgaira**[2,3], **Ernest G. Nolen**[4], **Gisela Cabré**[5], **Jordi Hernando**[5], **Dilip K. Tosh**[6], **Kenneth A. Jacobson**[6,*], **Concepció Soler**[2,3,*], **Francisco Ciruela**[1,2,*]

[1]Pharmacology Unit, Department of Pathology and Experimental Therapeutics, Faculty of Medicine and Health Sciences, Institute of Neurosciences, University of Barcelona, L'Hospitalet de Llobregat, Spain.

[2]Neuropharmacology and Pain Group, Neuroscience Program, Institut d'Investigació Biomèdica de Bellvitge, IDIBELL, L'Hospitalet de Llobregat, Spain.

[3]Immunology Unit, Department of Pathology and Experimental Therapeutics, Faculty of Medicine and Health Sciences, University of Barcelona, L'Hospitalet de Llobregat, Spain.

[4]Colgate University, Hamilton, NY, USA.

[5]Departament de Química, Universitat Autònoma de Barcelona, Cerdanyola del Vallès, Spain.

[6]Molecular Recognition Section, Laboratory of Bioorganic Chemistry, National Institute of Diabetes and Digestive and Kidney Diseases, National Institutes of Health, Bethesda, MD, USA.

Abstract

Psoriasis is a chronic and relapsing inflammatory skin disease lacking a cure that affects approximately 2% of the population. Defective keratinocyte proliferation and differentiation, and aberrant immune responses are major factors in its pathogenesis. Available treatments for moderate to severe psoriasis are directed to immune system causing systemic immunosuppression over time, and thus concomitant serious side effects (i.e. infections and cancer) may appear. In recent years, the G_i protein-coupled A_3 receptor (A_3R) for adenosine has been suggested as a novel and very promising therapeutic target for psoriasis. Accordingly, selective, and high affinity A_3R agonists are known to induce robust anti-inflammatory effects in animal models of autoimmune inflammatory diseases. Here, we demonstrated the efficacy of a selective A_3R
agonist, namely MRS5698, in preventing the psoriatic-like phenotype in the IL-23 mouse model of psoriasis. Subsequently, we photocaged this molecule with a coumarin moiety to yield the first photosensitive A_3R agonist, MRS7344, which in photopharmacological experiments prevented the psoriatic-like phenotype in the IL-23 animal model. Thus, we have demonstrated the feasibility of using a non-invasive, site-specific, light-directed approach to psoriasis treatment.

Graphical Abstract

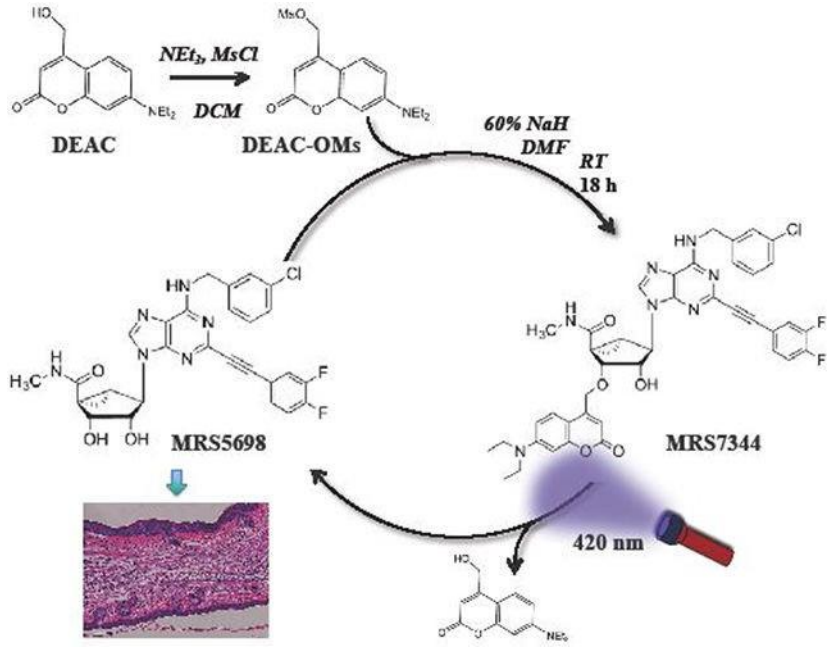

Keywords

psoriasis; anti-inflammatory; adenosine receptor; photopharmacology

1. Introduction

The immune system relies on complex interactions between cells and effector molecules to eliminate pathogenic agents through both innate and adaptive mechanisms. Indeed, disorders involving the immune system are challenging to treat pharmacologically without impacting other physiological processes, which can cause side effects.

The term psoriasis refers to a long-lasting immune-mediated disorder primarily characterized by cutaneous and systemic manifestations. Global psoriasis prevalence values fluctuate around 2% of the population, from which 70% to 80% present a mild variant, which is equally present in both sexes [1]. Although psoriasis mainly causes skin-related symptomatology (such as dryness, itchiness, scaly skin and abnormal skin patches and plaques), many other symptoms besides the skin-related may appear. Unfortunately, those comorbidities are associated with patients with chronic psoriasis, commonly affecting body joints as well as muscles and bones [1]. In addition, individuals with psoriasis have an increased risk of developing other chronic and serious health diseases, including psoriatic arthritis, cardiovascular disorders, Crohn's disease, and lymphoma. Although psoriatic lesions are able to appear in any skin region (including nails), typical locations have been reported [2]. Specifically, predilection sites include the extensor surfaces of forearms and shins, peri-umbilical, peri-anal, and retro-auricular regions and scalp. The psoriatic disease hallmarks rely on histopathological characteristics of diverse layers of the skin mucosa. Specifically, both epidermis and dermis are affected by the disease. In contrast to normal skin, psoriasis-injured epidermis develops three main features: i) epidermal acanthosis (i.e. thickening of viable layers), ii) hyperkeratosis (i.e. thickened cornified layer) and iii) parakeratosis (i.e. cell nuclei are present in the cornified layer). In addition, epidermal rete ridges (i.e. thickenings that extend down between dermal papillae) are markedly elongated. On the other hand, the subjacent layer, known as the dermis, presents dilated and contorted

blood vessels, which reach into the tips of the dermal papillae. In the dermis, an inflammatory infiltrate is produced involving neutrophils, dendritic cells, and T helper (Th) lymphocytes. Importantly, psoriasis pathogenesis onset and maintenance rely on a complex interplay between immune cells and keratinocytes, involving amplifying cytokine cascades. In particular, IL-23 (interleukin-23) and IL-12 released by inflammatory dendritic cells trigger differentiation and activation of Th17, Th1 and Th22 to produce IL-17, IFN-γ, TNF and IL-22 that impact keratinocyte proliferation and differentiation to increase skin thickness by inflammatory-dependent mechanisms [3].

Because psoriasis consists of a complex disease related to immune dysregulation, and this medical condition exclusively affects humans, there is a lack of both naturally occurring and virtual animal models mimicking the complex phenotype and pathogenesis of psoriatic disease. Nevertheless, numerous murine models of psoriasis have been generated over the past decades, as preclinical models [4]. Among the immunological reconstituted models in which local administration of several immune-related compounds (i.e. cytokines and interleukins) is used, is the IL-23-induced psoriatic-like phenotype mice model. This model relies on intradermal administration (i.e. into mouse ear dermis) of IL-23, which has been associated with skin swelling and psoriasis-like phenotype induction [5].

To date, because no psoriasis cure is available, treatments are focused on symptomatology management and based on general pharmacological groups (i.e., NSAIDs and immunosuppressants. There exist several high-quality evidence-based guidelines for psoriasis management [6]. These guidelines propose treatments for psoriatic lesions, as well as for disease progression. Needless to say, due to the complexity and intricate signal pathways of the immune system, immune drug-based therapies are extensively associated with the occurrence of severe adverse effects, especially when treatments involve immune- suppressant medications or chronic administration. However, in recent years, promising novel targets are being explored. An example is the use of non-immune system suppressant regulation factors, such as adenosine. Adenosine acts through four G protein-coupled receptor (GPCR) subtypes, all of which are of interest in treatment of chronic diseases, such as inflammation, by various pathways [7]. Interestingly, A_3R-selective agonist IB-MECA (CF101) is currently in advanced clinical trials as a potential therapeutic target for inflammatory diseases [7–9], and the receptor has been reported as a propitious drug-target for psoriatic-related disorders [10]. Here, we assess the efficacy of a new A_3R-selective agonist designed to be locally activated by light in the psoriatic lesioned skin.

2. Materials and methods

2.1. Synthesis of MRS7344

7-Diethylamino-4-hydroxymethylcoumarin (DEAC) was obtained from Indofine Chemical Co., Hillsborough, NJ. All reagents and solvents (regular and anhydrous) were of analytical grade and obtained from commercial sources. (1S,2R,3S,4R,5S)-4-(6-((3- Chlorobenzyl)amino)-2-((3,4-difluorophenyl)ethynyl)-9H-purin-9-yl)-2,3-dihydroxy-N- methylbicyclo[3.1.0]hexane-1-carboxamide (MRS5698) was synthesized as reported [17]. All reactions using anhydrous solvents were carried out under a nitrogen atmosphere using oven-dried glassware Thin-layer chromatography was performed using commercially prepared silica gel plates with a fluorescence indicator, and visualization was achieved with UV light (254 and 365 nm). Preparative chromatographic separations were performed on silica gel (0.040–0.063 mm). All NMR spectral assignments were determined by ^{1}H (400 or 500 MHz), ^{13}C (100 or 125 MHz) in $CDCl_3$ or CD_3OD. Peaks were referenced to residual chloroform signals (δH 7.26 ppm, or δC 77.0 ppm). High resolution mass spectra were recorded on a MALDI-TOF instrument.

The MRS7344 synthetic route is described in detail and summarized in Figure 1. In brief, to an ice-

water cooled solution of DEAC (50.0 mg, 0.202 mmol) in DCM (2.5 mL) was added sequentially triethylamine (56 µL, 0.40 mmol) and methanesulfonyl chloride (24 µL, 0.30 mmol), and the solution allowed to stir at 0–5 °C for 2 h. The reaction was quenched with cold saturated aqueous sodium bicarbonate diluted with DCM and separated, dried (Na_2SO_4) and concentrated in vacuo to give 64.4 mg, 98% of a yellow solid. ^{1}H NMR (400 MHz, chloroform-d) δ 7.34 (d, J = 9.0 Hz, 1H), 6.62 (dd, J = 9.1, 2.6 Hz, 1H), 6.54 (d, J = 2.6 Hz, 1H), 6.19 (t, J = 1.1 Hz, 1H), 5.32 (d, J = 1.1 Hz, 2H), 3.44 (q, J = 7.1 Hz, 4H), 3.13 (s, 3H), 1.23 (t, J = 7.1 Hz, 6H).

The following reaction was carried out in a dimly lit hood. To an ice-water cooled solution of MRS5698 (24.8 mg, 44 µmol) and DEAC-OMs (17.6 mg, 54 µmol) in 0.4 mL of anhydrous DMF under argon was added 60% NaH (2.0–2.4 mg, 84–100 µmol). The reaction was kept cold for 30 min, then stirred at rt overnight. After 18 h, the solvent was evaporated and co-distilled with toluene (3×), and the residue dried under high vacuum. The residue was taken up in 5% MeOH in DCM and applied to a preparative silica gel TLC plate (500 µm thickness) for separation using 50:1, EtOAc:MeOH. From the mixture, the yellow band at R_f 0.28 was collected to give 4.9 mg (14%) of the 3′-mono-alkylated material. The assignment of the 3′-hydroxyl group as the unambiguous site of the ether modification of MRS5698 was based on heteronuclear multiple bond correlation (HMBC) contacts between H3′ and both the amide carbonyl and the coumarin methylene (Fig. S1).

MALDI-TOF m/z cald for $C_{42}H_{38}ClF_2N_7O_5$ $[M + H]^+$ 794.27, found 794.28 and $[M + Na]^+$ 816.25, found 816.30. ^{1}H NMR (400 MHz, CD_3OD) δ 8.23 (s, 1H), 7.55 (m, 2H), 7.45 (m, 2H), 7.40–7.25 (m, 4H), 6.71 (dd, J = 9.0, 2.6 Hz, 1H), 6.51 (d, J = 2.6 Hz, 1H), 6.26 (t, J = 1.2 Hz, 1H), 5.01 (d, J = 6.4 Hz, 1H, H3′), H1′ peak obscured by H_2O in MeOD, 4.73 (dd, J = 14.7, 1.2 Hz, 1H), 4.45 (bdd, J = 6.4, 2.6 Hz, 1H, H2′), 3.47 (q, J = 7.1 Hz, 4H), 2.73 (s, 3H), 2.15 (dd, J = 8.8, 4.8 Hz, 1H), 1.91 (t, J = 5.2 Hz, 1H), 1.58 (m, 1H), 1.3 (t, J = 7.1 Hz, 6H).

2.2. Photochemical characterization

The uncaging process of MRS7344 was investigated by irradiating a 40 µM solution of this compound in phosphate buffered saline (PBS):DMSO 86:14 at 405 nm and 0.56 W cm^{-2} using a cw laser (MDL-E-405, Scitec Instruments Ltd., Wiltshire, UK). The changes observed in UV-vis absorption upon irradiation were monitored using a HP 8453 spectrophotometer (Agilent Technologies, Inc., Colorado Springs, CO, USA). Control experiments were conducted by irradiating MRS5698 and DEACM (Indofine Chemical Co., Hillsborough, NJ) solutions at the same conditions. From the UV-vis absorption measurements, the photouncaging quantum yield of MRS7344 was determined using the photoisomerization process of the closed state of 1,2-bis(5-chloro-2-methyl-3-thienyl)perfluorocyclopentene in hexane at 405 nm as a reference (Φ_{iso} = 0.13) [11,12].

2.3. Cell culture and stable transfection

Human embryonic kidney 293 (HEK-293) cells obtained from ATCC (American Type Culture Collection, Rockville, MD, USA; CRL-321, RRID: CVCL_0063) were grown in Dulbecco's modified Eagle's medium (DMEM) pre-heated at 37°C and supplemented with: 5% (v/v) fetal bovine serum (previously inactivated at 55°C for 30 min), 100 U/mL penicillin, 100 µg/mL streptomycin, 2 mM L-glutamine and non-essential amino acids. Manipulation and maintenance were done in a biological safety cabinet class 1 and in an incubator at 37°C, 5% CO_2 and 90% relative humidity. Absence of mycoplasma was checked regularly, thus only mycoplasma-free cells were used. HEK-293 cells were transfected with 10 µg of pIREShyg3-SP-HA-NL-A_3R plasmid (obtained from GenScript, Leiden, Netherlands), a cDNA encoding the human A_3R inserted in a vector containing the signal peptide of metabotropic glutamate receptor type 5 (i.e. SP), influenza hemagglutinin peptide (i.e. HA) and NanoLuc protein (i.e. NL).

Transfection was performed by using polyethylenimine (PEI) transfection reagent [13]. Then, 24 hours after transfection, cells were selected by seeding them in 60 cm^2 plates with supplemented DMEM in the presence of 0.1 mg/ml hygromycin for 3 weeks to enrich the percentage of cells expressing the receptor, thus ensuring its stable expression. As a result, HEK-293 cells stably expressing the human A_3R were used in pharmacological experiments.

2.4. cAMP accumulation inhibition assay

cAMP accumulation was measured using the LANCE Ultra cAMP kit following manufacturer's indications [14]. In brief, cells (8×10^5 cells/200µl) were firstly incubated with 2 mL of stimulation buffer consisting of DMEM supplemented with 0.1% BSA, adenosine deaminase (ADA, 0.5 U/ml) and the phosphodiesterase inhibitor zardaverine (100 µM) for 1 hour at 37°C and 300 rpm double orbital agitation. Subsequently, stimulation buffer was removed, and cells incubated with fresh stimulation buffer containing vehicle or the different drugs (i.e., MRS5698 and MRS7344), which were then continuous light-irradiated (or mock manipulated) with 420 nm wavelength light at 1.18 mW/cm^2 intensity LED. After 8 min, post-irradiated cells were challenged with forskolin (1 µM) for 30 min. Cells were plated at a 384-wells plate and Eu-cAMP tracer and ULight™-anti-cAMP reagents added. Cells were then incubated for 1 h in the dark at R.T. Thereafter, measurements at 620 nm and 665 nm were performed in a CLARIOstar Plus multi-mode microplate reader to determine cAMP levels following manufacturer's instructions. The results were expressed as the percentage of receptor (i.e. A_3R) activation induced by treatments following the equation:

$$\text{cAMP accumulation } \% = FV_{drug}/FV_{fsk} \times 100$$

Where FV_{drug} and FV_{fsk} represent the area FRET value in the drug+forskolin- and forskolin-treated conditions, respectively.

2.5. Animals

Adult C57BL/6N (Envigo Rms Spain SL., Sant Feliu de Codines, Spain) male and female mice bred in the animal facility of University of Barcelona (Campus of Bellvitge) weighing 25–35 g were used. The University of Barcelona Committee on Animal Use and Care (CEEA) approved the protocol. Following the approved experimental protocol all animals were supervised daily to assess signs of adverse effects during treatment. A retrospective analysis of the protocol demonstrated that no corrective measures (i.e. use of analgesics) were needed. Animals were housed and tested in compliance with the guidelines provided by the Guide for the Care and Use of Laboratory Animals [15] and following the European Union directives (2010/63/EU). Mice were housed in groups of five in standard cages with ad libitum access to food and water and maintained under a 12 h dark/light cycle (starting at 7:30 AM), at 22 °C and 66% humidity (standard conditions). All animal experimentation was carried out by a researcher blind to drug treatments.

2.6. IL23-induced psoriatic-like phenotype

The IL23-induced mouse model of psoriasis was performed using C57BL/6N mice, as previously described [5]. The experimental approach consisted in a 5 consecutive days protocol. Briefly, mice were anesthetized by the i.p. administration of a ketamine (100 mg/kg)/xylazine (10 mg/kg) mixture and ear thickness was measured using a digital calliper. Then recombinant mouse IL23 (500 ng) or PBS were i.d. injected into the ears by using a Hamilton syringe during three consecutive days (days 0, 1, and 2). At days 2 and 3 animals were treated intraperitoneally (i.p.) with vehicle (14.2% DMSO and 14.2% Tween80 in saline) or drugs (MRS5698 or MRS7344. 1mg/Kg) 20 min before being

anaesthetised. Light irradiation of the corresponding ear was conducted before IL-23 administration by using a custom-made 9 × 4 light-emitting diode (LED) matrix (12 × 9 cm) placed at a height of 8 cm above the animals' heads. Upon that approach, a 420 nm wavelength light regime consisted continuous light-irradiation at 1.18 mW/cm^2 intensity LED was performed during 8 min. Contralateral ear was covered in order to be protected from the collateral light-irradiation.

2.7. Histochemistry

Tissue samples from mice were fixed with 4% paraformaldehyde, embedded in paraffin and then cut in 5 μm sections. Sample processing for hematoxylin and eosin (H&E) staining was performed according to standard procedures [5].

2.8. Statistical analysis

GraphPad Prism 9.0.2 (San Diego, CA, USA) software was used for statistical analysis. Statistical significance was accepted when $P < 0.05$. Data are represented as mean ± standard error of mean (SEM). The number of samples/animals (n) in each experimental condition is indicated in the corresponding figure legend. Outliers were assessed by the ROUT method [16] assuming a Q value of 1% in GraphPad Prism 9.0.2. No animals were excluded. Comparisons among experimental groups were performed by Student's t test. Otherwise, statistical analysis was performed by one-way analysis of variance (ANOVA) followed by Bonferroni or Dunnett's multiple comparison post-hoc tests.

3. Results

3.1. Design and synthesis of a caged A_3R agonist

The A_3R-based ligand MRS7344, a caged derivative containing a violet light-absorbing coumarin, was designed and synthesized using MRS5698 [17] as a template. In brief, MRS7344 was synthesized by coupling one of the hydroxyl groups of MRS5698 to an O- methanesulfonyl derivative of the violet-light absorbing coumarin DEAC in a one-pot procedure (Fig. 1). The adenosine 2′ and 3′ hydroxyl groups are generally required for receptor binding, and the ribose binding region on the adenosine receptors is quite sterically restricted [18]. Thus, by reversibly blocking either or both of these hydroxyl groups the biological activity of adenosine agonists is expected to be prevented.

Once MRS7344 was synthesized and structurally validated, its photochemical properties were investigated. The absorption spectrum of MRS7344 in PBS:DMSO mixture (86:14, by volume) showed maxima at λ = 264, 317 and 383 nm that can be assigned to their separate MRS5698 and coumarin components (Fig. 2A). Because of the lack of absorption in the visible region of MRS5698, the photochemical behaviour of MRS7344 could be assessed upon selective excitation of its coumarin moiety by irradiation with 405 nm light. To this end, absorption spectral changes were concomitantly monitored, which showed a clear reduction of the coumarin absorption band under continuous illumination (Fig. 2B). These results are consistent with the photolysis of the coumarin benzylic bond and the release of the appended MRS7344 fragment [19,20]. For this process, a photo-uncaging quantum yield of Φ_{chem} = 0.013 was determined, which is in reasonable agreement with the photochemical behaviour reported for other biologically relevant hydroxyl groups caged with coumarins through an ether linkage [21,22].

3.2. Optical control of A_3R function in cultured cells

We assessed the light-dependent MRS7344-mediated A_3R activation by using classical cAMP

accumulation experiments in cells permanently expressing A_3R. To this end, we assessed the light-dependent MRS7344-mediated modulation of cAMP accumulation induced by A_3R activation. Thus, cells were incubated with forskolin before being challenged with increasing concentrations of a prototypical A_3R full agonist (i.e., MRS5698) or of the new photocaged A_3R agonist (i.e., MRS7344) and under different irradiation conditions (Fig. 3). As expected, agonist challenge (MRS5698) induced a robust A_3R-mediated cAMP reduction, regardless the illumination condition (Fig. 3A). Thus, MRS5698 induced comparable [$F_{(1,36)}$ = 0.4628, P = 0.5007] nanomolar concentration- dependent effect both in dark (pIC_{50}= 8.02 ± 0.12) and light (pIC_{50}= 8.18 ± 0.15) conditions (Fig. 3A). Of note, MRS5698 did not inhibited forskolin-induced cAMP accumulation in non-transfected HEK-293 cells (Fig. 3A, black triangles). Conversely, although MRS7344 was unable to inhibit forskolin-induced cAMP accumulation in dark conditions (Fig. 3B, black circles), it elicited concentration-dependent cAMP effects, equivalent to MRS5698, upon 405 nm visible light-irradiation, thus displaying nanomolar potency (pIC_{50}= 7.81 ± 0.18) comparable to that observed for MRS5698 (pIC_{50}= 8.18 ± 0.15; [$F_{(1,36)}$ = 1.538, P = 0.2230] (Fig. 3B, blue circles).

3.3. *Light-dependent efficacy of* **MRS7344** *in the IL-23 mouse model of psoriasis*

Once MRS7344 light-dependent activity was validated in living cells, we aimed to assess its efficacy in a well-established animal model of psoriasis disease. Accordingly, the IL-23- induced psoriasis-like preclinical model of inflammation was implemented [23]. Briefly, recombinant mouse IL-23 interleukin was injected (i.d.) into the mouse ears following a consecutive paradigm (i.e., once daily for 3 days). Ears intradermally injected with PBS were used as control. Subsequently, ear thickness was measured daily using a digital calliper as an indication of the course of progression toward psoriasis (Fig. 4A). As expected [24], intradermal mouse ear injection of IL-23 induced marked swelling compared with PBS (Fig. 4B, left panel). The administration of MRS5698 during the second and third day after the first IL-23 injection, significantly (P = 0.001) reduced the IL-23 induced ear thickness during the third and fourth experimental days (Fig. 4B, middle panel). Conversely, under the same experimental conditions MRS7344 was unable to prevent the IL23-induced ear inflammation (Fig. 4B, right panel). Importantly, when the ear of a MRS7344-treated animal was illuminated with 420 nm light during 8 min after each MRS7344 administration, a significant (P = 0.0001) reduction of IL-23-induced ear inflammation was observed during the third and fourth experimental days (Fig. 4B, right panel, blue circles). In addition, no anti-inflammatory effect was observed in the contralateral to illumination ear of an animal treated with MRS7344 (Fig. 4B, right panel, black circles), thus suggesting the lack of systemic diffusion of MRS5698 upon photorelease. Of note, the illumination regime of IL-23 administered ears (blue symbols) from animals treated with either vehicle (triangles) or MRS5698 (squares) did not alter the expected result, thus demonstrating that ear light irradiation neither affected IL-23-induced inflammation nor the MRS5698-mediated anti- psoriatic effect, respectively (Fig. 4B, left and middle panels). Accordingly, H&E staining (Fig. 5) showed reduced thickness and immune cell infiltration in the IL23-treated ears of MRS5698-treated and MRS7344-treated/irradiated mice compared to the IL23-treated ears of vehicle-treated mice and MRS7344-treated/non-irradiated mice (Fig. 5, right panels, arrows). On the other hand, no significant differences among drug treatments were observed in IL23-induced keratinocyte hyperplasia (number of epidermal layer) (Fig. S2), suggesting major effects of the A_3R agonist in the activation of psoriatic-driven immune cells rather than in keratinocyte proliferation. Overall, these results are indicative that MRS7344 photo-uncaging occurred in intradermal tissue upon non-toxic, non-invasive topical irradiation of the mouse ear, thus releasing MRS5698 locally and precluding IL-23-induced inflammation.

4. Discussion

In the present work, we characterized a photocaged compound for the treatment of psoriasis, a common chronic inflammatory skin disease that requires treatment over a patient's lifetime. Unfortunately, in spite of the increasing understanding of the molecular players, signalling pathways and cellular basis involved in the pathogenesis of psoriasis, no cure currently exists.

Depending on the variant and severity of psoriasis, different therapies are prescribed. For low to mild or highly focalized and located skin lesions, topical therapies are available, whereas for high severity subtypes or those widely spread over the skin and diffuse, systemic drug treatments are commonly prescribed. Of note, most of the local and systemic therapies target the immune system in a gross (e.g., glucocorticoids, methotrexate and cyclosporine) or relatively specific (e.g., antibodies against TNF-α, IL-23 and IL-17, cytokines responsible of the inflammatory phenotype) manner. Thus, both treatment categories are usually associated with the appearance of unwanted immunosuppressive side- effects, including the risk of liver and kidney dysfunction, infection and cancer. Moreover, some patients are or become non-responders to current therapies [1,25]. Indeed, due to these side effects and limitations, novel therapies are urgently needed. In recent years, the A_3R has been suggested as a novel and very promising therapeutic target for psoriasis and other inflammatory conditions [7]. Thus, numerous A_3R agonists, partial agonists, antagonists, and allosteric modulators have been studied, culminating in the development of potent and selective molecules. The A_3R has been found to be upregulated in peripheral blood mononuclear cells (PBMCs) obtained from patients affected by different autoimmune disorders such as rheumatoid arthritis, Crohn's disease, and psoriasis [7]. Interestingly, A_3R agonism has been shown to induce important anti-inflammatory effects in several cellular and animal models [26–33]. Furthermore, the results achieved with A_3R agonists in clinical studies are quite promising. Thus, the prototypical A_3R selective agonist methyl 1-[N^6-(3- iodobenzyl)-adenin-9-yl]-β-D-ribofuronamide (IB-MECA, Piclodenoson) is in clinical trials for inflammation, showing safety and clinical efficacy in earlier Phases I and II trials [34]. Indeed, IB-MECA has entered larger Phase III trials for rheumatoid arthritis and psoriasis [9,10,34,35]. However, one difficulty in developing adenosine receptor drugs is the ubiquitous expression of ARs within an organism leading to side effects, and A_3R agonists are no exception. Based on clinical trials with the systemic application of an A_3R agonist by oral administration, widespread or serious adverse effects would not be expected. However, a case of hyponatremia was observed in a patient receiving Cl-IB-MECA (25 mg BID dose) as 2nd-line treatment for advanced hepatocellular carcinoma and moderate hepatic dysfunction [36]. Also, IB-MECA (2 mg BID dose) in a clinical trial for plaque psoriasis was noted to cause infections and gastrointestinal events [35]. Consequently, here we used MRS7344, derived from MRS5698, as a light-dependent, highly selective agonist of A_3R, able to be photoactivated in a tissue- and time-controlled manner. The A_3R selectivity compared to other adenosine receptors of the liberated drug MRS5698 is >3000-fold, and its drug-likeness was established in preclinical testing [17]. The site of reversibly masking the nucleoside with a coumarin ether was chosen according the expectation that the receptor- bound ribose moiety is surrounded by a conserved, polar and sterically restricted region on the A_3R, based on X-ray crystal and cryo-EM structures of the nucleoside agonist-bound, closely related A_1 and A_{2A} receptors [18,37]. The approach of using light to activate drugs by photoisomerization, photosensitization or photocleavage for treating dermatological conditions, such as skin cancer and pain, is especially appealing [38–40]. There are numerous examples of photodynamic therapy for skin conditions, but our approach of unmasking a potent, bioactive receptor ligand specifically on the skin by cleaving a photolabile group is uncommon [20,41].

We initially investigated the basic characteristics and photoreactivity of the molecule (i.e., irradiation time). Subsequently, we evaluated light-dependent effects of MRS7344 in HEK cells stably expressing the A_3R. Accordingly, we evaluated the pharmacological activity of MRS7344 monitoring intracellular cAMP levels changes. Interestingly, MRS7344 was able to dose-dependently inhibit forskolin-mediated cAMP intracellular accumulation upon 420 nm light irradiation. Thus, we obtained similar efficacy to that obtained for the parent drug, MRS5698. Once the light-dependent effects of MR7344 were ascertained in a heterologous system, we aimed at examining its pharmacological activity within the IL-23 psoriatic mouse model. A remarkable advantage of this model resides in its ability to be replicated. Additionally, each of the animal's ears can be treated with a different compound (or eventually vehicle) or even different light schedules (i.e., illuminating one ear and mock manipulating the other), thus allowing the use of one animal as both the experimental subject and the internal negative control. Interestingly, MRS7344 demonstrated anti- psoriatic-like efficacy in a light-dependent fashion and upon non-toxic non-invasive topical procedure. The obtained anti-inflammatory outcomes were comparable to those observed for MRS5698 treatment. Indeed, further MRS7344 pharmacological studies, including pharmacokinetics and bioavailability, upon oral administration would be necessary before any potential therapeutic exploration. Also, it would be interesting to compare topical administration (i.e., unguent) of different MRS7344 doses and photoactivation duration according to pathology severity. Overall, the photopharmacological approach using MRS7344 demonstrated similar benefits to that observed when using a specific monoclonal antibody (i.e. anti-IL-23) or employing genetically manipulated animals [42,43].

In conclusion, we have used a photocleavable masking group, a coumarin ether, to clearly demonstrate a proof of concept of using light to unmask a potent and selective receptor (GPCR) ligand for skin treatment. Noteworthy, while A_1R and $A_{2A}R$ agonists may lead to important cardiovascular side effects, A_3R agents display a better therapeutic index and tolerability, which may be suitable for the treatment of psoriasis, among other neuroinflammatory-related syndromes [44]. Indeed, by using photocaged compounds [45] the drug would be even safer, totally avoiding possible cardiovascular effects. Nevertheless, it would be important to further examine these putative secondary effects, in order to establish a safe approach based on the use of A_3R light-dependent drugs.

Acknowledgements

This work was supported by FEDER/Ministerio de Ciencia, Innovación y Universidades– Agencia Estatal de Investigación (SAF2017-87349-R to FC and SAF2017-83815-R to CS) and ISCIII (PIE14/00034), the Catalan government (2017 SGR 1604), Fundació la Marató de TV3 (Grant 20152031), FWO (SBO-140028) to FC, the intramural funds of the National Institute on Drug Addiction, and the NIDDK Intramural Research Program (ZIADK31117). We thank Centres de Recerca de Catalunya (CERCA) Programme/Generalitat de Catalunya for IDIBELL institutional support. We thank Esther Castaño and Benjamín Torrejón from the Scientific and Technical Services (SCT) group at the Bellvitge Campus of the University of Barcelona for their technical assistance.

References

[1]. Greb JE, Goldminz AM, Elder JT, Lebwohl MG, Gladman DD, Wu JJ, Mehta NN, Finlay AY, Gottlieb AB, Psoriasis, Nat. Rev. Dis. Prim. 2 (2016) 1–17. doi:10.1038/nrdp.2016.82.

[2]. Dopytalska K, Sobolewski P, Błaszczak A, Szymańska E, Walecka I, Psoriasis in special localizations, Reumatologia. 56 (2018) 392–398. doi:10.5114/reum.2018.80718.

[3]. Lowes MA, Suárez-Fariñas M, Fariñas F, Krueger JG, Immunology of Psoriasis, (2014). doi:10.1146/annurev-

immunol-032713-120225.

[4]. Wagner EF, Schonthaler HB, Guinea-Viniegra J, Tschachler E, Psoriasis: What we have learned from mouse models, Nat. Rev. Rheumatol. 6 (2010) 704–714. doi:10.1038/nrrheum.2010.157.

[5]. Manils J, Casas E, Viña-Vilaseca A, López-Cano M, Díez-Villanueva A, Gómez D, Marruecos L, Ferran M, Benito C, Perrino FW, Vavouri T, de Anta JM, Ciruela F, Soler C, The Exonuclease Trex2 Shapes Psoriatic Phenotype, J. Invest. Dermatol. 136 (2016) 2345–2355. doi:10.1016/ j.jid.2016.05.122.

[6]. Stiff KM, Glines KR, Porter CL, Cline A, Feldman SR, Current pharmacological treatment guidelines for psoriasis and psoriatic arthritis, Expert Rev. Clin. Pharmacol. 11 (2018) 1209–1218. doi:10.1080/17512433.2018.1548277.

[7]. Jacobson KA, Merighi S, Varani K, Borea PA, Baraldi S, Aghazadeh Tabrizi M, Romagnoli R, Baraldi PG, Ciancetta A, Tosh DK, Gao ZG, Gessi S, A_3 Adenosine Receptors as Modulators of Inflammation: From Medicinal Chemistry to Therapy, Med. Res. Rev. 38 (2018) 1031–1072. doi:10.1002/med.21456.

[8]. David M, Akerman L, Ziv M, Kadurina M, Gospodinov D, Pavlotsky F, Yankova R, Kouzeva V, Ramon M, Silverman MH, Fishman P, Treatment of plaque-type psoriasis with oral CF101: Data from an exploratory randomized phase 2 clinical trial, J. Eur. Acad. Dermatology Venereol. 26 (2012) 361–367. doi:10.1111/j.1468-3083.2011.04078.x.

[9]. Yiu ZZN, Warren RB, Novel Oral Therapies for Psoriasis and Psoriatic Arthritis, Am. J. Clin. Dermatol. 17 (2016) 191–200. doi:10.1007/s40257-016-0179-3.

[10]. Borea PA, Gessi S, Merighi S, Vincenzi F, Varani K, Pharmacology of adenosine receptors: The state of the art, Physiol. Rev. 98 (2018) 1591–1625. doi:10.1152/physrev.00049.2017.

[11]. Lees AJ, A Photochemical Procedure for Determining Reaction Quantum Efficiencies in Systems with Multicomponent Inner Filter Absorbances, Anal. Chem. 68 (1996) 226–229. doi:10.1021/ ac9507653.

[12]. Higashiguchi K, Matsuda K, Asano Y, Murakami A, Nakamura S, Irie M, Photochromism of Dithienylethenes Containing Fluorinated Thiophene Rings, European J. Org. Chem. (2005) 91–97.

[13]. Longo PA, Kavran JM, Kim M-S, Leahy DJ, Transient mammalian cell transfection with polyethylenimine (PEI), Methods Enzymol. 529 (2013) 227–240. doi:10.1016/B9780-12-418687-3.00018-5.

[14]. Taura J, Nolen EG, Cabré G, Hernando J, Squarcialupi L, López-Cano M, Jacobson KA, Fernández-Dueñas V, Ciruela F, Remote control of movement disorders using a photoactive adenosine A_{2A} receptor antagonist. J. Control. Release. 283 (2018) 135–142. doi:10.1016/ j.jconrel.2018.05.033.

[15]. Clark JD, Gebhart GF, Gonder JC, Keeling ME, Kohn DF, Special Report: The 1996 Guide for the Care and Use of Laboratory Animals., ILAR J. 38 (1997) 41–48.

[16]. Motulsky HJ, Brown RE, Detecting outliers when fitting data with nonlinear regression - A new method based on robust nonlinear regression and the false discovery rate, BMC Bioinformatics. 7 (2006). doi:10.1186/1471-2105-7-123.

[17]. Tosh DK, Padia J, Salvemini D, Jacobson KA, Efficient, large-scale synthesis and preclinical studies of MRS5698, a highly selective A_3 adenosine receptor agonist that protects against chronic neuropathic pain, Purinergic Signal. 11 (2015) 371–387. doi:10.1007/s11302-015-9459-2.

[18]. Xu F, Wu H, Katritch V, Han GW, Jacobson KA, Gao ZG, Cherezov V, Stevens RC, Structure of an agonist-bound human A_{2A} adenosine receptor, Science. 332 (2011) 322–327. doi:10.1126/ science.1202793.

[19]. Givens RS, Rubina M, Wirz J, Applications of p-hydroxyphenacyl (pHP) and coumarin-4- ylmethyl photoremovable protecting groups, Photochem. Photobiol. Sci. 11 (2012) 472–488. doi:10.1039/c2pp05399c.

[20]. Klán P, Šolomek T, Bochet CG, Blanc A, Givens R, Rubina M, Popik V, Kostikov A, Wirz J, Photoremovable protecting groups in chemistry and biology: reaction mechanisms and efficacy, Chem. Rev. 113 (2013) 119–91. doi:10.1021/cr300177k.

[21]. Tang S, Cannon J, Yang K, Krummel MF, Baker JR, Choi SK, Spacer-Mediated Control of Coumarin Uncaging for Photocaged Thymidine, J. Org. Chem. 85 (2020) 2945–2955. doi:10.1021/acs.joc.9b02617.

[22]. Wong PT, Roberts EW, Tang S, Mukherjee J, Cannon J, Nip AJ, Corbin K, Krummel MF, Choi SK, Control of an Unusual Photo-Claisen Rearrangement in Coumarin Caged Tamoxifen through an Extended Spacer, ACS Chem. Biol. 12 (2017) 1001–1010. doi:10.1021/acschembio.6b00999.

[23]. Singh TP, Zhang HH, Hwang ST, Farber JM, IL-23- and Imiquimod-Induced Models ofExperimental Psoriasis in Mice, Curr. Protoc. Immunol. 125 (2019). doi:10.1002/cpim.71.

[24]. Nakajima K, Sano S, Mouse models of psoriasis and their relevance, J. Dermatol. 45 (2018) 252–263. doi:10.1111/1346-8138.14112.

[25]. Armstrong AW, Read C, Pathophysiology, Clinical Presentation, and Treatment of Psoriasis: A Review, JAMA - J. Am. Med. Assoc. 323 (2020) 1945–1960. doi:10.1001/jama.2020.4006.

[26]. Antonioli L, Csóka B, Fornai M, Colucci R, Kókai E, Blandizzi C, Haskó G, Adenosine and inflammation: what's new on the horizon?, Drug Discov. Today. 19 (2014) 1051–1068. doi:10.1016/j.drudis.2014.02.010.

[27]. Borea PA, Gessi S, Merighi S, Varani K, Adenosine as a Multi-Signalling Guardian Angel in Human Diseases: When, Where and How Does it Exert its Protective Effects?, Trends Pharmacol. Sci. 37 (2016) 419–434. doi:10.1016/j.tips.2016.02.006.

[28]. Gessi S, Merighi S, Stefanelli A, Fazzi D, Varani K, Borea PA, A_1 and A_3 adenosine receptors inhibit LPS-induced hypoxia-inducible factor-1 accumulation in murine astrocytes, Pharmacol. Res. 76 (2013) 157–170. doi:10.1016/j.phrs.2013.08.002.

[29]. Cunha RA, Different cellular sources and different roles of adenosine: A_1 receptor-mediated inhibition through astrocytic-driven volume transmission and synapse-restricted A_{2A} receptor- mediated facilitation of plasticity, Neurochem. Int. 52 (2008) 65–72. doi:10.1016/ j.neuint.2007.06.026.

[30]. Haskó G, Szabó C, Németh ZH, Kvetan V, Pastores SM, Vizi ES, Adenosine receptor agonists differentially regulate IL-10, TNF-alpha, and nitric oxide production in RAW 264.7 macrophages and in endotoxemic mice, J. Immunol. 157 (1996) 4634–4640.

[31]. Szabó C, Scott GS, Virág L, Egnaczyk G, Salzman AL, Shanley TP, Haskó G, Suppression of macrophage inflammatory protein (MIP)-1α production and collageninduced arthritis by adenosine receptor agonists, Br. J. Pharmacol. 125 (1998) 379–387. doi:10.1038/sj.bjp.0702040.

[32]. Haskó G, Németh ZH, Vizi ES, Salzman AL, Szabó C, An agonist of adenosine A_3 receptors decreases interleukin-12 and interferon-γ production and prevents lethality in endotoxemic mice, Eur. J. Pharmacol. 358 (1998) 261–268. doi:10.1016/S0014-2999(98)00619-0.

[33]. Mabley J, Soriano F, Pacher P, Haskó G, Marton A, Wallace R, Salzman A, Szabó C, The adenosine A_3 receptor agonist, N^6-(3-iodobenzyl)-adenosine-5′-N-methyluronamide, is protective in two murine models of colitis, Eur. J. Pharmacol. 466 (2003) 323–329. doi:10.1016/S0014-2999(03)01570-X.

[34]. Fishman P, Bar-Yehuda S, Liang BT, Jacobson KA, Pharmacological and therapeutic effects of A_3 adenosine receptor agonists, Drug Discov. Today. 17 (2012) 359–366. doi:10.1016/ j.drudis.2011.10.007.

[35]. David M, Gospodinov DK, Gheorghe N, Mateev GS, Rusinova MV, Hristakieva E, Solovastru LG, V Patel R, Giurcaneanu C, Hitova MC, Purcaru AI, Horia B, Tsingov II, Yankova RK, Kadurina MI, Ramon M, Rotaru M, Simionescu O, Benea V, Demerdjieva ZV, Cosgarea MR, Morariu HS, Michael Z, Cristodor P, Nica C, Silverman MH, Bristol DR, Harpaz Z, Farbstein M, Cohen S, Fishman P, Treatment of Plaque-Type Psoriasis With Oral CF101: Data from a Phase II/III Multicenter, Randomized, Controlled Trial, J. Drugs Dermatology. 15 (2016) 931–938.

[36]. Stemmer SM, Manojlovic NS, Marinca MV, Petrov P, Cherciu N, Ganea D, Ciuleanu TE, Pusca IA, Beg MS, Purcell WT, Croitoru AE, Ilieva RN, Natošević S, Nita AL, Kalev DN, Harpaz Z, Farbstein M, Silverman MH, Bristol D, Itzhak I, Fishman P, Namodenoson in advanced hepatocellular carcinoma and Child–Pugh B cirrhosis: Randomized placebo-controlled clinical trial, Cancers (Basel). 13 (2021) 1–12. doi:10.3390/cancers13020187.

[37]. Draper-Joyce CJ, Khoshouei M, Thal DM, Liang Y-L, Nguyen ATN, Furness SGB, Venugopal H, Baltos J-A, Plitzko JM, Danev R, Baumeister W, May LT, Wootten D, Sexton PM, Glukhova A, Christopoulos A, Structure of the adenosine-bound human adenosine A_1 receptor-G_i complex, Nature. 558 (2018) 559–563. doi:10.1038/s41586-018-0236-6.

[38]. Iseppon F, Arcangeletti M, Optogenetics and photopharmacology in pain research and therapeutics, STEMedicine. 1 (2020) e43.

[39]. Muniyandi K, George B, Parimelazhagan T, Abrahamse H, Role of Photoactive Phytocompounds in Photodynamic Therapy of Cancer, Molecules. 25 (2020). doi:10.3390/molecules25184102.

[40]. Hüll K, Morstein J, Trauner D, In Vivo Photopharmacology, Chem. Rev. 118 (2018) 10710–10747. doi:10.1021/acs.chemrev.8b00037.

[41]. Lerch MM, Hansen MJ, van Dam GM, Szymanski W, Feringa BL, Emerging Targets in Photopharmacology, Angew. Chemie. 55 (2016) 10978–99. doi:10.1002/anie.201601931.

[42]. Rizzo HL, Kagami S, Phillips KG, Kurtz SE, Jacques SL, Blauvelt A, IL-23– Mediated Psoriasis- Like Epidermal Hyperplasia Is Dependent on IL-17A, J. Immunol. 186 (2011) 1495–1502. doi:10.4049/jimmunol.1001001.

[43]. Singh S, Kroe-Barrett RR, Canada KA, Zhu X, Sepulveda E, Wu H, He Y, Raymond EL, Ahlberg J, Frego LE, Amodeo LM, Catron KM, Presky DH, Hanke JH, Selective targeting of the IL23 pathway: Generation and characterization of a novel highaffinity humanized anti-IL23A antibody, mAbs 7 (2015) 778–791. doi:10.1080/19420862.2015.1032491.

[44]. Janes K, Symons-Liguori AM, Jacobson KA, Salvemini D, Identification of A_3 adenosine receptor agonists as novel non-narcotic analgesics, Br. J. Pharmacol. 173 (2016) 1253–1267. doi:10.1111/bph.13446.

[45]. Silva JM, Silva E, Reis RL, Light-triggered release of photocaged therapeutics - Where are we now?, J. Control. Release. 298 (2019) 154–176. doi:10.1016/j.jconrel.2019.02.006.

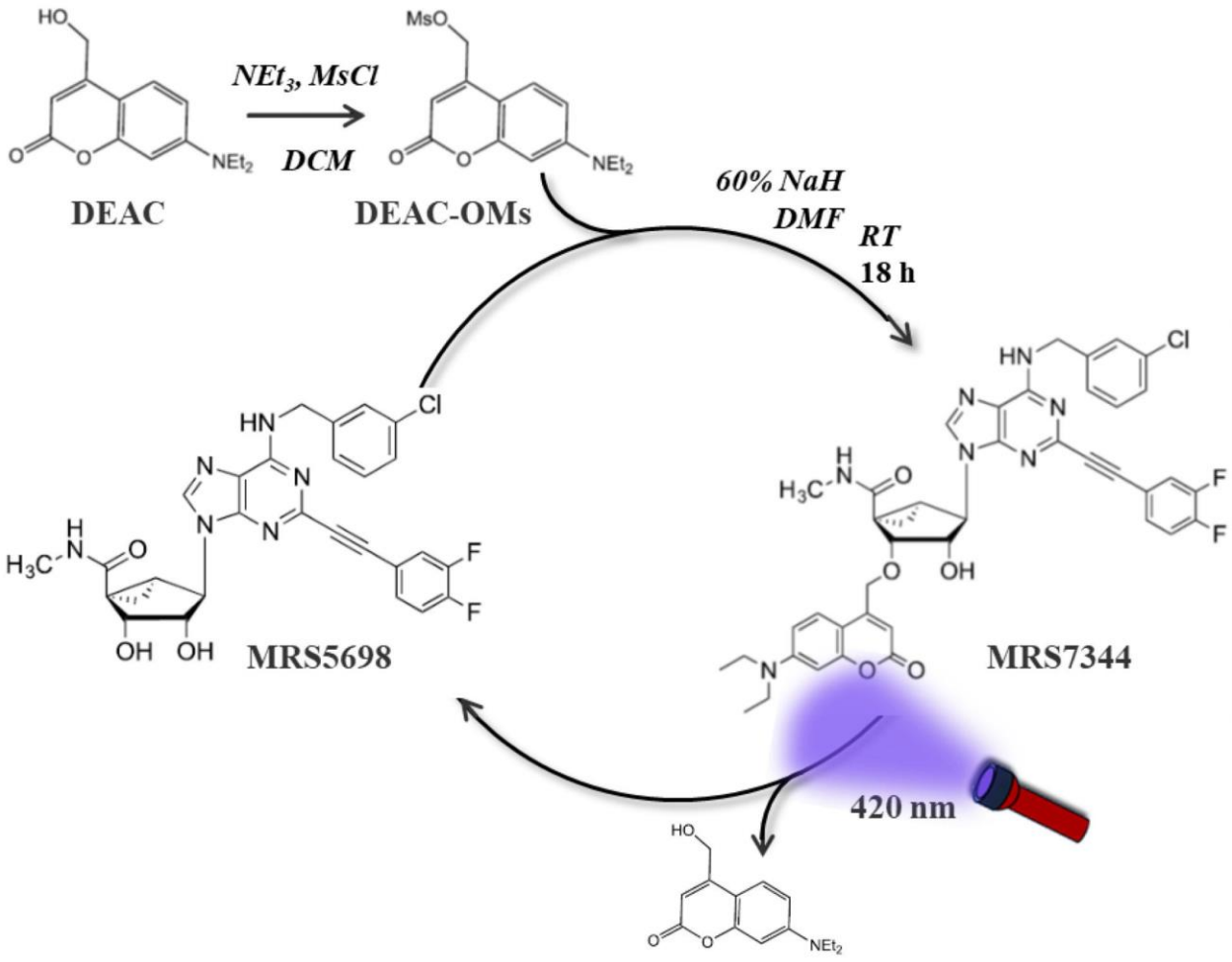

Figure 1. Design, synthesis, and photo-uncaging of MRS7344.
The synthesis of MRS7344 involves a procedure using MRS5698 and 7-diethylamino-4-hydroxymethylcoumarin (DEAC). Upon irradiation with 420 nm visible light the irreversible photolytic reaction produced MRS5698.

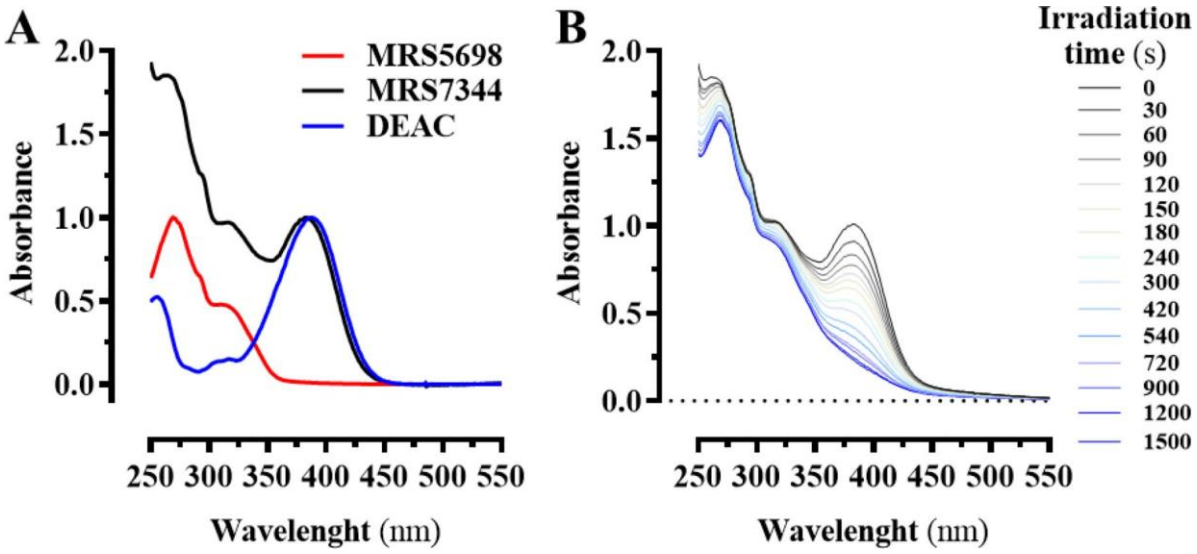

Figure 2. Photochemical properties of MRS7344.
(**A**) Absorption spectra of MRS7344 and its separate MRS5698 and DEAC units in PBS:DMSO 86:14 (c = 40 μM). (**B**) Variation of the absorption spectrum of MRS7344 in PBS:DMSO 86:14 (c = 40 μM) upon continuous irradiation at 405 nm (0.56 W/cm^2; irradiation time = 0–25 min).

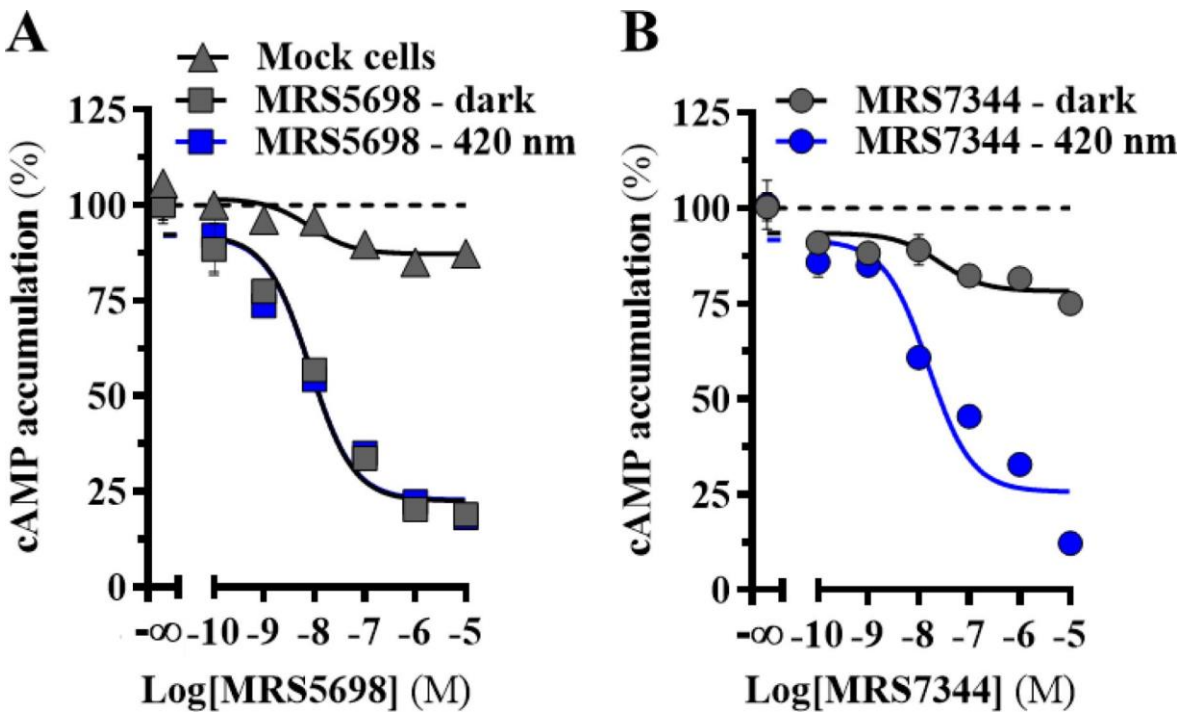

Figure 3. Determination of A_3R-mediated inhibition of intracellular cAMP accumulation in HEK cells.

HEK-293T cells permanently expressing the A_3R were incubated with increasing concentrations (from 0.1 nM to 10 μM) of MRS5698 (A, squares) and MRS7344 (B, circles) in dark conditions (black symbols) or upon 420 nm light irradiation (blue symbols). In addition, non-transfected HEK-293 cells (mock cells) were treated with increasing concentrations of MRS5698 (A, triangle) in dark conditions and the cAMP accumulation determined. The percentage of cAMP accumulation was calculated as described in materials and methods. The data are expressed as the mean ± SEM of three independent experiments performed in triplicate.

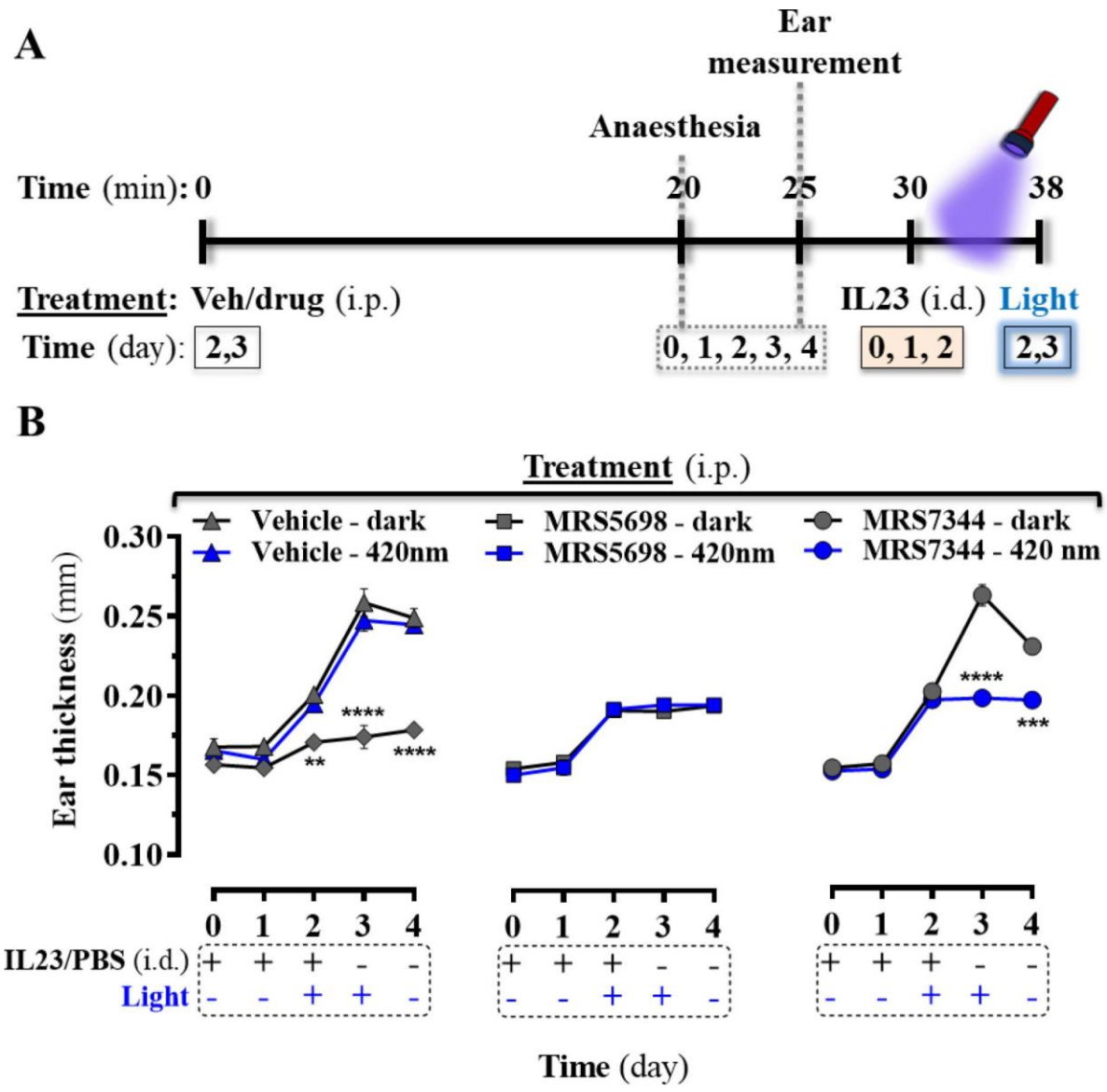

Figure 4. IL-23-induced psoriatic phenotype in C57BL/6 mice.

(A) Temporal scheme for IL-23-induced mouse model of psoriasis. The ear thickness of animals was measured upon anaesthesia every single day for the 5-day duration of the protocol. Animals were treated with IL-23 (i.d.) in both ears during three consecutive days (day 0, 1 and 2). At day 2 and 3 animals were previously intraperitoneally (i.p.) administered with vehicle (Veh, 14.2 % DMSO + 14.2% Tween80 in saline) and drugs (i.e., MRS5698 and MRS7344). When indicated the left animal's ear was irradiated with 420 nm light at day 2 and 3. **(B)** Mice ear thickness determinations. At day 2 and 3 IL-23 (i.d.) treated mice were administrated (i.p.) with vehicle (left panel, triangles), MRS5698 (1 mg/kg; middle panel, squares) or MRS7344 (1 mg/kg; right panel, circles) before the left ear was irradiated at 420 nm for 8 min (day 2 and 3, blue symbols) whereas right ear was covered to keep it in dark conditions and used as animal internal control of IL-23 mediated inflammation (black symbols). In addition, a contralateral control was performed consisting in a group of animals intradermally injected (day 0, 1 and 2) with IL-23 in the left ear and with PBS in the right ear while its thickness was monitored overtime (left panel, black rhombus). Ear thickness was measured in millimeters (mm) and shown as mean ± S.E.M., n = 5 mice per group. Similar results were obtained in three independent experiments using male and female.****P < 0.0001. ***P < 0.001 and **P < 0.01 Student's t test.

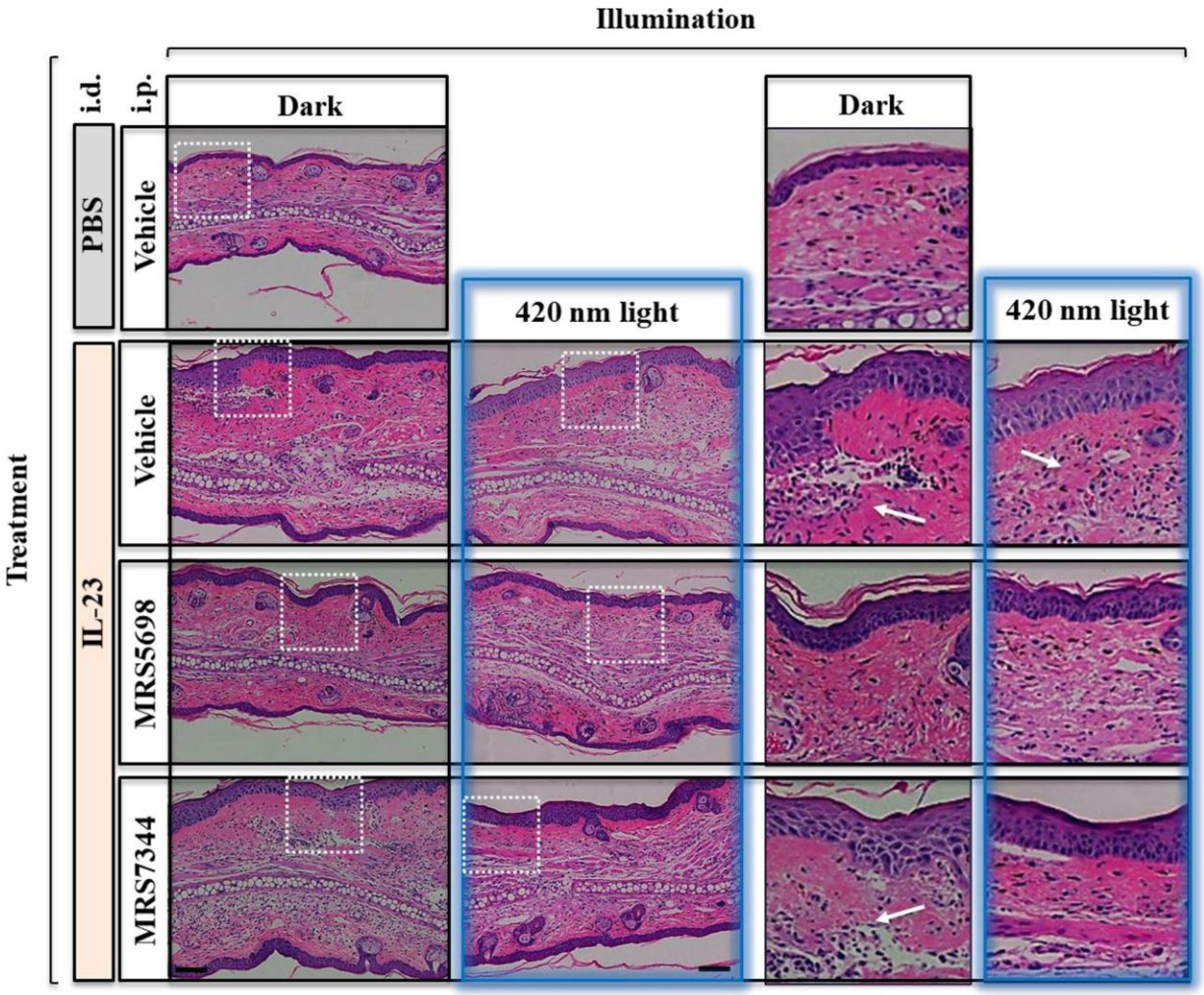

Figure 5. IL-23-induced psoriatic phenotype in C57BL/6 mice.
Representative H&E-stained ear sections of IL-23-treated mice from each experimental group shown in Figure 4. A magnification of the indicated ear region (dashed white square) is shown. Arrows indicate infiltrated immune cells, mainly neutrophils. Scale bars: 100 μm.